AIP | Physics of Fluids

Vortex tube reconnection at Re = 104

Wim M. van Rees, Fazle Hussain, and Petros Koumoutsakos

Citation: Phys. Fluids **24**, 075105 (2012); doi: 10.1063/1.4731809
View online: http://dx.doi.org/10.1063/1.4731809
View Table of Contents: http://pof.aip.org/resource/1/PHFLE6/v24/i7
Published by the American Institute of Physics.

Vortex tube reconnection at $Re = 10^4$

Wim M. van Rees,[1] Fazle Hussain,[2] and Petros Koumoutsakos[1,a)]
[1]*Institute of Computational Science, ETH Zürich, Zürich, Switzerland*
[2]*Department of Mechanical Engineering, University of Houston, Houston, Texas 77204, USA*

(Received 11 April 2012; accepted 8 June 2012; published online 11 July 2012)

We present simulations of the long-time dynamics of two anti-parallel vortex tubes with and without initial axial flow, at Reynolds number $Re = \Gamma/\nu = 10^4$. Simulations were performed in a periodic domain with a remeshed vortex method using 785×10^6 particles. We quantify the vortex dynamics of the primary vortex reconnection that leads to the formation of elliptical rings with axial flow and report for the first time a subsequent collision of these rings. In the absence of initial axial flow, a $-5/3$ slope of the energy spectrum is observed during the first reconnection of the tubes. The resulting elliptical vortex rings experience a coiling of their vortex lines imparting an axial flow inside their cores. These rings eventually collide, exhibiting a $-7/3$ slope of the energy spectrum. Studies of vortex reconnection with an initial axial flow exhibit also the $-7/3$ slope during the initial collision as well as in the subsequent collision of the ensuing elliptical vortex rings. We quantify the detailed vortex dynamics of these collisions and examine the role of axial flow in the breakup of vortex structures.
 [http://dx.doi.org/10.1063/1.4731809]

I. INTRODUCTION

The reconnection of vortex tubes is an archetypal problem of fluid dynamics. Repeated vortex reconnections have been postulated as a driving mechanism for turbulence and aerodynamic noise generation[1] and the destruction of aircraft wakes.[2,3] In recent years, studies of vortex reconnection have been central to the question of singularity formation of the Euler and Navier-Stokes equations.[4–8]

Experimental studies of vortex reconnection include the pioneering works of Refs. 9–12 for the collision of two vortex rings. A number of simulations, predominantly based on spectral methods, have described the different phases of the reconnection process for Re in the range 1000–3500. These studies include reconnections of vortex rings,[13–16] anti-parallel tubes,[17–20] anti-parallel tubes with an orthogonal offset[21–24] as well as other configurations leading to interesting topological dynamics.[15,25,26] The head-on collision of two vortex rings has been studied experimentally and numerically.[27–31] A theoretical model of vortex reconnection was proposed by Saffman,[32] and has been critically evaluated against numerical simulations by Boratav *et al.*[24] for the case of two orthogonal vortex tubes, and by Shelley *et al.*[20] for the case of two anti-parallel vortex tubes. A review of several of these works has been presented by Kida.[33]

Recently Hussain and Duraisamy[34] presented results of vortex reconnection up to $Re = 9000$. This work described the early time behavior of the vortices, limited to the first collision of the vortex tubes. In this paper we extend these simulations not only by studying a higher $Re = 10\,000$, but also by performing these simulations for longer times revealing for the first time the dynamics of the vortices after their first collision. We quantify the governing mechanisms and identify an important role of the axial flow (helicity) imparted to the vortex structures after their primary collision that governs their subsequent evolution. Furthermore in order to quantify the effects of axial flow in vortex reconnection we study the vortex reconnection process with an initially imposed axial flow.

a)Electronic mail: petros@ethz.ch.

We observe a $-7/3$ slope in the energy spectrum in all cases where an axial flow is present during vortex collisions.

The paper is organized as follows: in Sec. II we detail the computational setup of our simulations. Section III explains the flow evolution without initial axial flow organized around the different phases in the flow. Section IV presents the effects of initial axial flow on vortex reconnection, and in Sec. IV C we discuss the results of the simulations. We present our conclusions in Sec. V.

II. COMPUTATIONAL METHODS

Simulations are performed in the velocity ($\mathbf{u}$) – vorticity ($\boldsymbol{\omega} \equiv \nabla \times \mathbf{u}$) form of the incompressible Navier-Stokes equations

$$\nabla \cdot \mathbf{u} = 0, \tag{1}$$

$$\frac{\partial \boldsymbol{\omega}}{\partial t} + \mathbf{u} \cdot \nabla \boldsymbol{\omega} = \boldsymbol{\omega} \cdot \nabla \mathbf{u} + \nu \nabla^2 \boldsymbol{\omega}, \tag{2}$$

where ν is the kinematic viscosity. These equations are discretized using a remeshed vortex method[35,36] as employed for massively parallel computer architectures.[37–40]

We simulate the flow in a periodic domain with dimensions $[3\pi \times 4\pi \times 2\pi]$ centered at (0, 0, 0) and an underlying mesh of $[960 \times 1280 \times 640]$ computational elements. The vorticity field is initialized to an axisymmetric profile[18]

$$\omega(r) = \begin{cases} \omega_0 \left[1 - \exp\left(-\frac{K}{r^*} \exp\left(\frac{1}{r^* - 1}\right)\right)\right] & \text{if } r^* < 1, \\ 0 & \text{else,} \end{cases} \tag{3}$$

where $r^* = r/r_{\text{cutoff}}$ with $r_{\text{cutoff}} = 0.666$, and $K = 1/2\exp(2)\log(2)$. Along the z-direction the tubes are sinusoidally perturbed with an amplitude A and an inward inclination angle α to force their collision by self-induction. For the vortex tube in the negative half of the x-plane, the core location is

$$r(\mathbf{x})^2 = [x - (x_c + A\cos(\alpha)(1 + \cos(z)))]^2 + [y - (y_c + A\sin(\alpha)(1 + \cos(z)))]^2, \tag{4}$$

where $x_c + 2A\cos(\alpha)$ and $y_c + 2A\sin(\alpha)$ are the x- and y-coordinates of the center of the vortex tube in the $z = 0$ plane. The vorticity field of this tube is given by[41,42]

$$\boldsymbol{\omega}(\mathbf{x}) = \omega(r)\left(-A\cos(\alpha)\sin(z)\mathbf{e_x} - A\sin(\alpha)\sin(z)\mathbf{e_y} + \mathbf{e_z}\right). \tag{5}$$

Here $\mathbf{e_x}$, $\mathbf{e_y}$, and $\mathbf{e_z}$ are the unit vectors in x-, y-, and z-directions, respectively.

The space between the unperturbed tubes in the $z = \pi$-plane is 1.732 and we set $A = 0.2$, $\alpha = \pi/3$ for the tube in the negative half of the x-plane, and $\alpha = 2\pi/3$ for the other. Time is non-dimensionalized as $t = t^*\omega_0/20$, where ω_0 is the peak vorticity at $t^* = 0$. The $Re \equiv \Gamma/\nu = 10\,000$ is based on the initial circulation of one unperturbed tube. The initial vorticity field is rendered divergence free by a solenoidal reprojection.

The axial flow imposed initially on the tubes (see Sec. IV) is based on an axisymmetric velocity profile (similar to the vorticity profile)

$$u_z(r) = \begin{cases} u_0 \left[1 - \exp\left(-\frac{K}{r^*} \exp\left(\frac{1}{r^* - 1}\right)\right)\right] & \text{if } r^* < 1, \\ 0 & \text{else,} \end{cases} \tag{6}$$

where $r^* = r/r_{\text{cutoff}}$ with $r_{\text{cutoff}} = 0.666$. The corresponding azimuthal vorticity distribution is

$$\omega_\theta(r) = \begin{cases} -\frac{u_0}{0.666}\left[\frac{K(r^{*2} - r^* + 1)}{(r^* - 1)^2 r^{*2}} \exp\left(\frac{1}{r^* - 1} - \frac{K}{r^*} \exp\left(\frac{1}{r^* - 1}\right)\right)\right] & \text{if } r^* < 1, \\ 0 & \text{else.} \end{cases} \tag{7}$$

The vorticity field obtained by adding this azimuthal vorticity component to the axial vorticity component is perturbed according to Eq. (4).

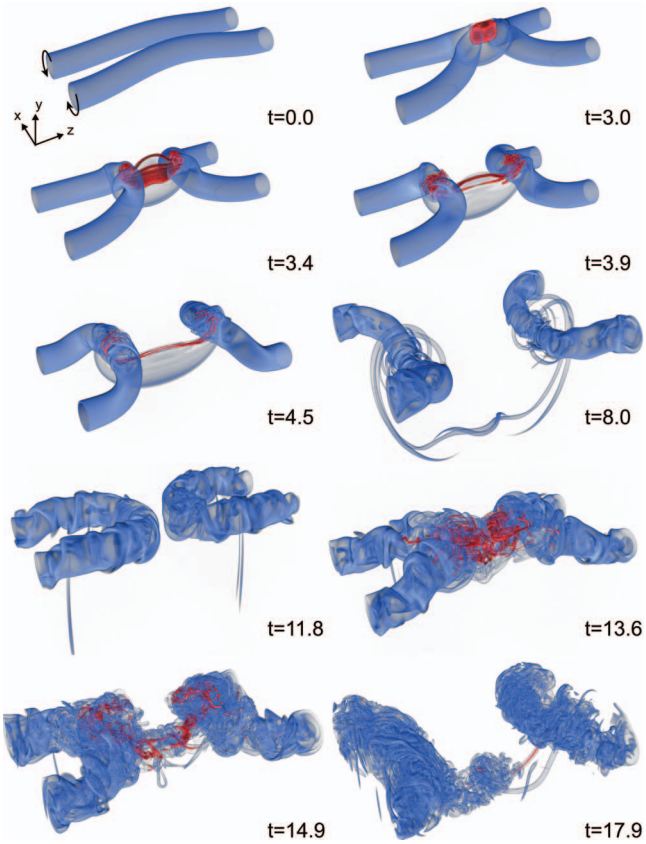

FIG. 1. Volume rendering of vorticity magnitude at specified times. Light and dark gray (blue and red online) are centered around values of $0.4\omega_0$ and $3.75\omega_0$, respectively.

The accuracy of the simulations is quantified by the effective viscosity, defined as the ratio of the time decay of total energy and the total enstrophy,[43] which does not exceed 2% in all simulations. The results of the remeshed vortex methods for the reconnection without axial flow agree well with those of pseudo-spectral simulations. The reader is referred to van Rees *et al.*[40] for a comparison of pseudo-spectral and remeshed vortex methods.

III. VORTEX RECONNECTION OF TUBES WITHOUT INITIAL AXIAL FLOW

The collision of the vortex tubes entails the distinct stages of: (a) the first vortex tube collision followed by (b) a quiescent evolution of the resulting elliptical vortex rings during which an axial flow is imparted to their core by the coiling of the vortex lines, and (c) the ensuing collision of the elliptical vortex rings. Visualizations of the vorticity field for all stages are shown in Figure 1.

A. First collision

The vortex tubes approach and collide starting at $t = 2.5$. The tubes are flattened in the collision area forming two anti-parallel vortex sheets. Viscous cross-diffusion annihilates the circulation at the contact point and circulation transfers from the symmetry plane to the dividing plane (Figure 2, left), leading to the formation of elliptical vortex rings. Similar to simulations at $Re = 10^3$,[18] the connected transverse vortex lines pile up to form the transverse vorticity structures (*bridges*), and remnant circulation is organized into two parallel elongated structures (*threads*) consisting of vortex lines that did not undergo reconnection. As opposed to the lower *Re* case,[18] here the threads roll up around the bridges (Figure 5(a)) and acquire high vorticity due to their stretching by the bridges.

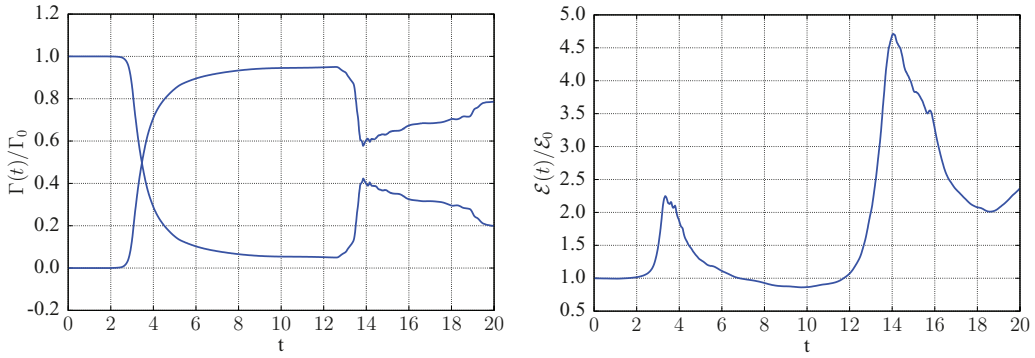

FIG. 2. (Left) Circulation in half of the planes defined by $x = 0$ (dividing plane) and $z = 0$ (symmetry plane) as a function of time, normalized by the circulation in the $z = 0$ plane at $t = 0$. (Right) Evolution of enstrophy over time, normalized by its value at $t = 0$.

Simultaneously, under mutual induction of adjacent bridges, the ends of the newly created vortex rings move up and away from each other. During this first phase of the reconnection process, the enstrophy increases to more than twice its initial value (Figure 2, right).

We report for the first time a $-5/3$ slope in the energy spectrum of the flow (Figure 3, left). While at $t = 0$ most energy is concentrated at the smallest wavenumbers, corresponding to the length scales of the tubes and the core diameters, at $t = 3.4$ we see a large increase in the small-scale energy and the spectrum exhibits distinct power-law and viscous regimes. The power-law regime with $-5/3$ slope is manifested as soon as the tubes first touch at $t = 2.5$. At $t = 3.1$ the $-5/3$ slope is fully established in slightly less than a decade of intermediate wavenumbers and remains at these levels until $t = 3.4$. At later times the energy in the high wavenumbers gradually decays by dissipation and we can no longer identify distinct power-law and viscous regimes.

With the first collision an axial flow is imparted on the core of the newly formed rings. This flow is directed away from the bridges, as visualized in Figure 4 by the helicity density in a moving reference frame $\boldsymbol{\omega} \cdot (\mathbf{u} - \mathbf{U})$, where, following Kida *et al.*,[16] $\mathbf{U}$ is given by

$$\mathbf{U} = \left(0, \frac{\int (\boldsymbol{\omega} \cdot \mathbf{u}) \omega_2 \, \mathrm{d}V}{\int (\omega_2)^2 \, \mathrm{d}V}, 0 \right)^T . \tag{8}$$

In order to elucidate the establishment of the axial flow we visualize the evolution of the vorticity field by instantaneous vortex lines in Figure 5. The lines in the primary reconnection region are rolled

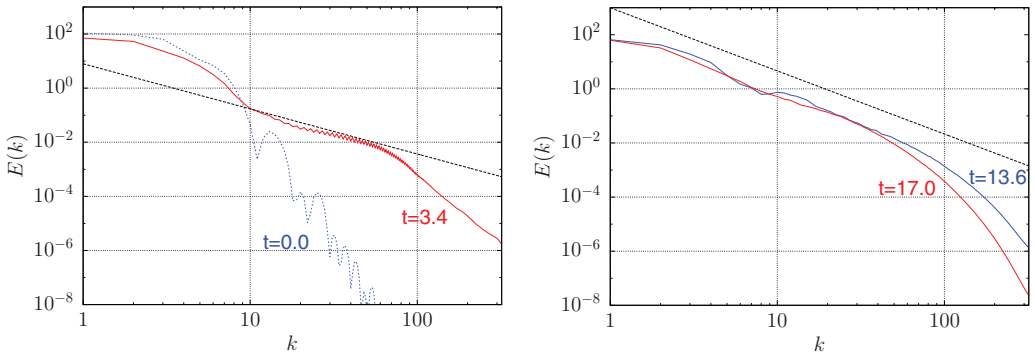

FIG. 3. Three-dimensional energy spectrum of the case without initial axial flow. (Left) $t = 0$ and $t = 3.4$. (Right) $t = 13.6$ and $t = 17.0$. The straight dashed lines correspond to a $-5/3$ slope in the left plot, a $-7/3$ slope in the right plot.

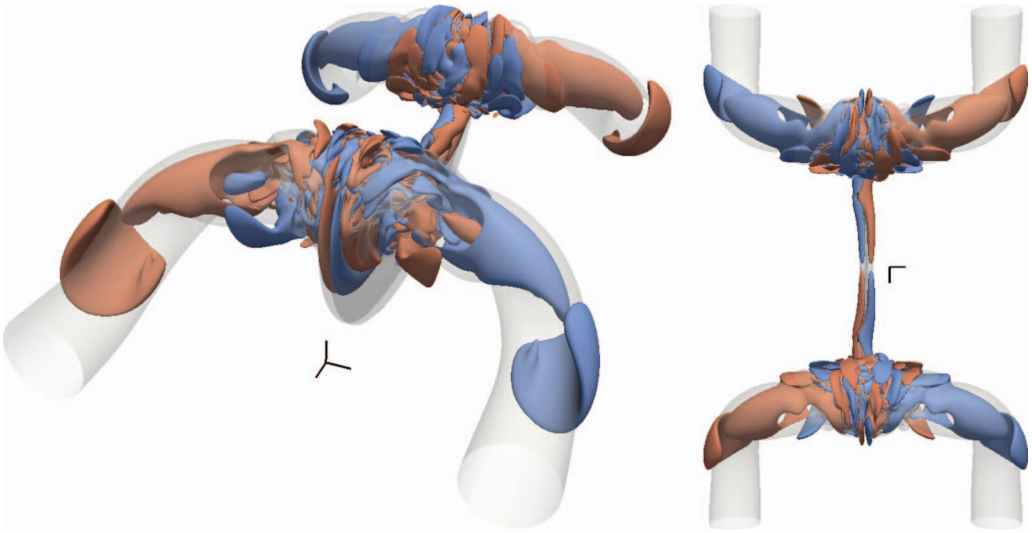

FIG. 4. Two isosurfaces of $\boldsymbol{\omega} \cdot (\mathbf{u} - \mathbf{U})$ at $\pm 2\%$ of its maximum value at $t = 4.5$. Perspective view (left) and top view (right) with negative (light gray, blue online) and positive (dark gray, red online) isosurfaces and transparent isosurface of $|\boldsymbol{\omega}| = 0.5\omega_0$ (gray).

up by the swirl of the bridges. The intense vorticity of the threads induces in turn axial flow within the bridges away from the initial plane of symmetry[18] (Figure 4).

B. Quiescent period

The quiescent period between $t = 4.0$ and $t = 12.0$ involves the evolution of the elliptical vortex rings (Figure 6). At first, the rings have their major axes aligned with the z-direction. The ends of the threads, remnants of the first collision, wrap around the bridges. In this phase, the vorticity magnitude in these threads is much lower than in the bridges. Helical waves on the rings can be observed: first single waves traveling away from the connection region, and then several co-existing helical waves of opposite directionality. The elliptic vortex rings undergo an oscillation, switching axes, such that at $t \approx 12$ their major axes are again aligned with the z-direction.

We note that the energy dissipation after the collision follows a decay law of the form

$$\frac{\partial E}{\partial t} \propto -t^{-(p+1)}, \tag{9}$$

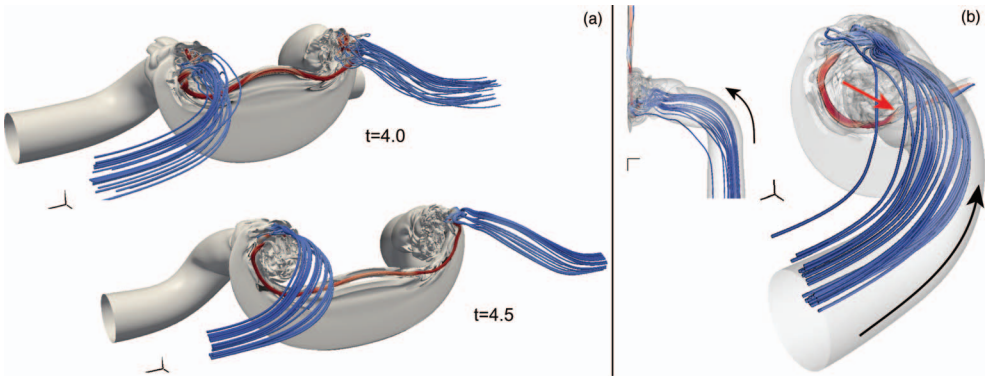

FIG. 5. (a) Vortex lines and isosurface of $|\boldsymbol{\omega}| = 0.5\,\omega_0$ (solid gray). The vortex lines, colored by $|\boldsymbol{\omega}|$, are seeded from regions where $|\boldsymbol{\omega}| > 7.0\,\omega_0$ and are drawn only for $\boldsymbol{\omega} > 0.25\,\omega_0$. (b) Directions of vorticity (black arrows) and axial flow (gray arrow, red online) for the $x > 0$ and $z > 0$ quarter of the domain at $t = 4.5$.

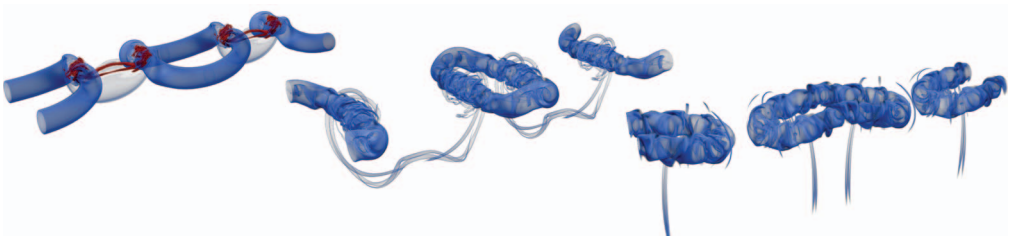

FIG. 6. Volume renderings of vorticity magnitude plotted for $t = 3.0$ (left); $t = 5.4$ (middle); and $t = 8.4$ (right). Two periods in z-direction are shown, the colormap is as in Figure 1.

where p is in the range $p = 1.2$–1.4 (Figure 7), similar to the energy decay rate found in fully developed turbulence, where $1.0 \lesssim p \lesssim 1.4$ (Kolmogorov[44] and discussion in Lesieur[45]). This result is consistent with observations made by Kida *et al.*[16] despite the much lower Re of 1000 of that study.

The axial flow in the core of the rings, originally directed away from the connection region (Figure 4), changes its direction as the rings separate. A second reversal of the axial flow is observed starting at $t = 6.5$, such that it is again directed away from the connection region. For simplicity we represent the quarter ring in the $x > 0$ and $z > 0$ part of the domain by a straight vortex tube (Figure 8), with the left end corresponding to the location of the bridge and the right end corresponding to the undisturbed end of the ring. Without any axial vorticity variation the vortex lines are straight (uncoiled) and no axial flow is imparted on the cores. After the collision, however, the vorticity in the bridges is stronger than the vorticity farther away, leading to a right-handed polarization of the vortex lines and hence an axial flow directed from right to left (middle of Figure 8), i.e., towards the bridges. Subsequently, as the rings oscillate due to axes switching, the vorticity magnitude decreases in the bridges and increases at the undisturbed ends, consistent with elliptical vortex ring dynamics.[46] The situation then resembles the right panel of Figure 8: a left polarization of the vortex lines is established, imparting an axial flow directed away from the bridges. Note that in an experimental study on vortex rings,[47] an axial flow inside the ring was also found, and attributed to the presence of an axial vorticity gradient.

In order to further demonstrate the development of the axial flow we apply a helical wave decomposition (HWD) (Refs. 45 and 48) to the vorticity field, which decomposes the field into the sum of a right-handed and a left-handed component: $\boldsymbol{\omega}(\mathbf{x}) = \boldsymbol{\omega}_R(\mathbf{x}) + \boldsymbol{\omega}_L(\mathbf{x})$. The HWD has been applied before in studies of helical turbulence.[49] Here we follow the approach of previous studies on vortex dynamics using the HWD.[50,51] If the vorticity field is unpolarized, there is no preferred handedness in the vortex lines and the left- and right-handed components of the vorticity field will have equal magnitudes. Following *Virk et al.*,[51] a scalar measure of the local handedness of the

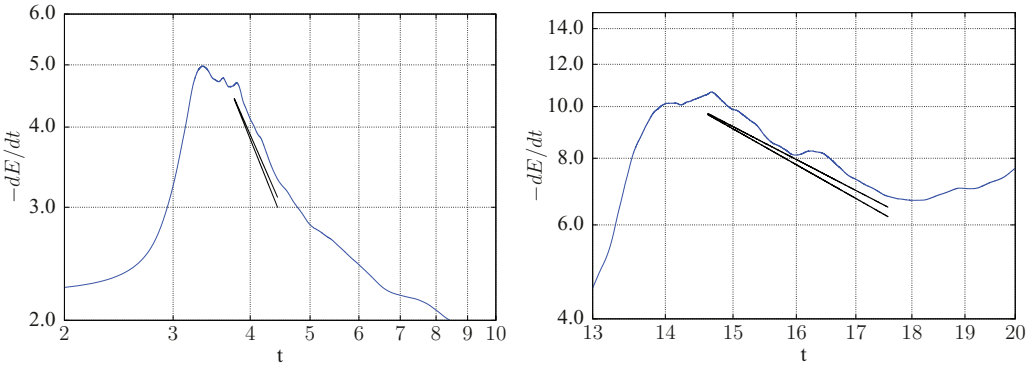

FIG. 7. Energy decay after the first (left) and second (right) reconnection, on a log-log scale. The two solid lines in each panel denote slopes of -2.2 and -2.4, respectively.

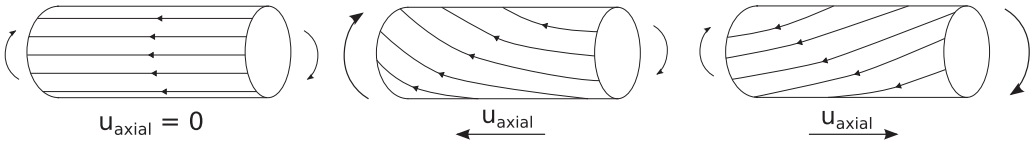

FIG. 8. The effect of an axial vorticity gradient in the core of a vortex tube. Reference configuration (no axial flow) with constant vorticity and parallel vortex lines (left). A configuration with stronger vorticity on the left side gives rise to a right-handed polarization in the vortex lines and an axial flow from right to left (middle). A stronger vorticity on the right side gives rise to a left-handed polarization in the vortex lines and an axial flow from left to right (right).

vorticity field is

$$R_a(\mathbf{x}) = \log_2\left(\frac{|\boldsymbol{\omega}_R|}{|\boldsymbol{\omega}_L|}\right),$$

where $\boldsymbol{\omega}_R$ and $\boldsymbol{\omega}_L$ are the right- and left-handed components of the vorticity field, respectively.

Figure 9 visualizes isosurfaces of R_a. In the quarter of the domain where $x > 0$ and $z > 0$, at $t = 4.5$ we observe a structure of negative R_a at the reconnection region, corresponding to the polarization of the vortex lines drawn in Figure 5. An axial flow away from the bridges confirms our analysis in Sec. III A. Between $t = 4.5$ and $t = 5.5$ an isosurface of positive R_a (indicated by a black arrow at $t = 4.5$–5.5) grows helically from the connection region. This structure corresponds to a dominant right-handed vorticity field which imparts an axial flow towards the bridge region, as explained in the middle panel of Figure 8. For $t \geq 6.5$ (Figure 9) a left-handed structure emerges in the outer end of the vortex core at $x > 0$, $z > 0$—with an axial flow away from the reconnection region, as sketched in the right panel of Figure 8 and visualized by the helicity density in Figure 10.

During the quiescent phase we observe a secondary-level vortex collision between the threads (see Figure 11). A third thread-like structure is visible, emanating from the bridges and wrapping around the main threads. The vorticity field reminds one of the connection between two tubes of unequal strength.[52,53] However, because of the low local *Re* of the threads ($Re = 550$), the vorticity in the threads diffuses without any significant circulation transfer. One may argue that a higher initial *Re* will increase the local thread *Re* so that a reconnection between the threads could be enabled. We note however that here the remnant circulation relative to the initial circulation is lower than that observed for vortex tube collision at $Re = 1000$ (Ref. 18), so that the thread *Re* may increase only slowly with increasing initial *Re*. Furthermore, as observed also in Hussain and Duraisamy,[34] the threads are sensitive to a Kelvin-Helmholtz instability due to their stretching by the bridges, so that they are more likely to break up earlier at higher Reynolds numbers.

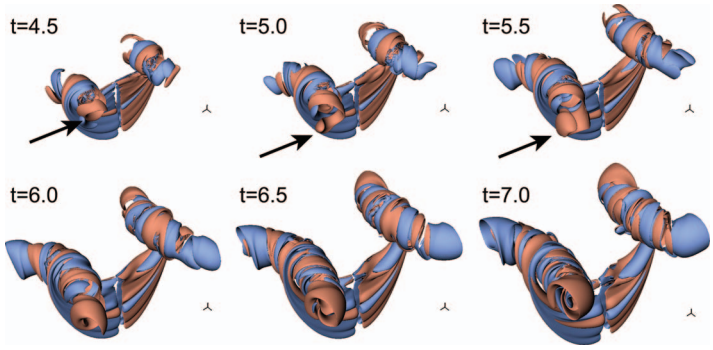

FIG. 9. Isosurfaces of R_a between $t = 4.5$ and $t = 7.0$. Each isosurface is colored by its sign (positive dark (red online), negative light (blue online)) and their values are $R_a = \pm 0.5$. The arrows at $t = 4.5$–5.5 indicate the right-polarized structure that expands along the tube.

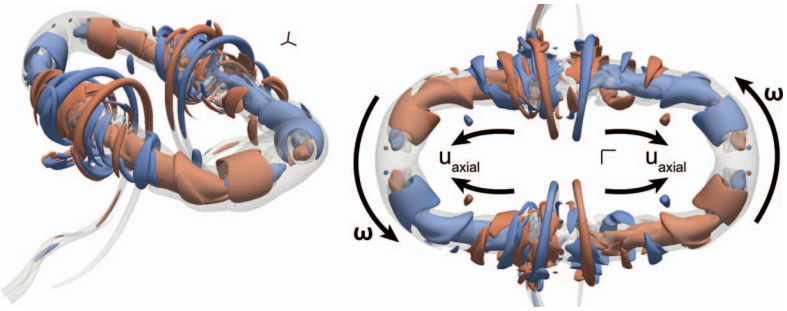

FIG. 10. Isosurfaces of positive (dark gray, red online) and negative (light gray, blue online) values of $\boldsymbol{\omega} \cdot (\mathbf{u} - \mathbf{U})$ at $t = 7.0$, for the same value as Figure 4, plotted with a periodic image to show one full ring. We show a perspective view (left) and a top view (right), where we annotated the visualization with directions of vorticity and axial flow. A transparent isosurface of $|\boldsymbol{\omega}| = 0.5\omega_0$ is shown in gray.

C. Second collision

After their build up and initial oscillatory evolution, the elliptical rings approach each other and collide at $t = 12$. The collision is associated with a burst of small-scale vortical structures with large vorticity magnitudes in the region where the two rings meet. During this collision, circulation is transferred by the onset of a reconnection. However, after about 40% of the circulation has been transferred, the process stops at $t = 13.6$. We note that the second collision starts almost simultaneously with the new oscillation cycle of the rings. The ends of the rings moving away from each other due to axis-switching would explain the shorter and smaller circulation transfer.

The energy spectrum during and after this second collision (Figure 3, right) exhibits a power-law regime, now with a $-7/3$ slope present over more than a decade of wavenumbers from $t = 14.5$ to $t = 22.0$. We report further on the energy spectrum in Sec. IV C, where we relate it to our observations from vortex collision with initial axial flow presented in Sec. IV.

For $t > 14$ we observe two large clusters of small-scale structures that move apart, similar to the motion of the bridges in the first collision. Two vortex tubes connecting these clusters are visible, surrounded by small-scale vorticity generated during the last collision. These tubes remind one of the threads containing the remnant circulation after the collision between the initial tubes. However, we note that since the vortex tubes are the topologically new structures, the word "threads" should actually refer to the large-scale structures. These large clusters are expected to undergo further oscillations and further collisions as they evolve, transferring energy to smaller scales with each collision as the flow evolves towards a turbulent state.

IV. RESULTS WITH INITIAL AXIAL FLOW

To study the effect of an initial axial flow in the tubes, we simulated the flow with two different initial swirl numbers: $q = 0.383$ (case 1) and $q = 0.958$ (case 2). Here q is defined as $q = u_0/u_{\theta,0}$, where u_0 is the prefactor in Eq. (6), corresponding to the peak axial flow strength in the tube, and

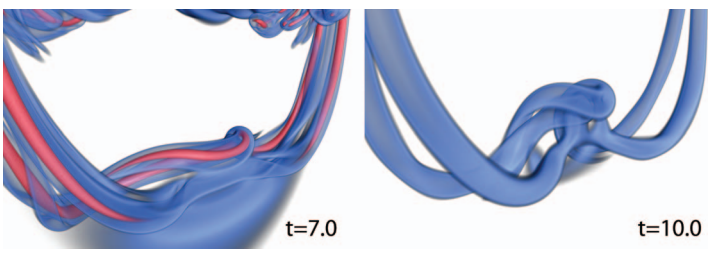

FIG. 11. Volume renderings of vorticity magnitude showing the remnant threads from the first connection at the specified times. The light and dark grays (blue and red online) are centered around values of $0.14\omega_0$ and $0.8\omega_0$, respectively.

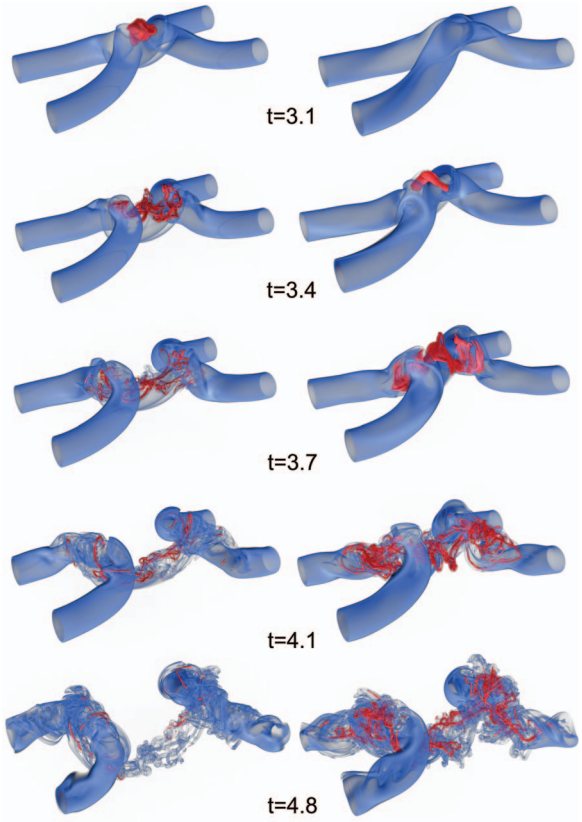

FIG. 12. Volume rendering of vorticity magnitude for case 1 (left column) and case 2 (right column) at the specified times. The colormap is the same as in Figure 1.

$u_{\theta,0} = \|\mathbf{u}_{(t=0)} \cdot \mathbf{e}_\theta\|_\infty$ is the peak azimuthal velocity of an unperturbed tube at $t = 0$. We discuss case 1 and case 2 separately, and refer to the simulation without initial axial flow as case 0. Flow visualizations of both case 1 and case 2 are presented in Figure 12.

A. Case 1: $q = 0.383$

At the onset of the first collision, the tubes flatten in the midplane to form two vortex sheets like a plane jet, with each half having an oblique velocity due to the opposing axial flow. In contrast to case 0 (Figure 1), the vortex sheet now shears and undergoes a Kelvin-Helmholtz instability, accompanied by a large spike in vorticity magnitude and the rapid transfer of energy to smaller scale vorticity structures. A helical perturbation travels on one half of each of the newly connected structures, convected by the axial flow that is transferred from the initial anti-parallel tubes to the newly created elliptical rings. The remnant circulation of the collision is contained in several small-scale vortical structures. The value of the peak enstrophy is almost unchanged with respect to case 0 (Figure 13, right), indicating that the main differences in the vorticity fields between these two cases (i.e., with and without axial flow) are of local nature.

We observe a larger rate and a larger amount of circulation transfer in case 1 (Figure 14, left), whereas its onset is slightly later than in case 0. These differences are quantified by the maximum circulation transfer rate $\mathrm{d}\Gamma^*/\mathrm{d}t$, where $\Gamma^* = \Gamma/\Gamma_0$ and Γ_0 is the circulation in the symmetry plane at $t = 0$, and $t_{\mathrm{d}\Gamma^*/\mathrm{d}t,\max}$, the time of maximum circulation transfer rate (Table I). We also show the reconnection time t_R according to the definition given in Ref. 34 where $t_R = t_{0.5} - t_{0.95}$: the time needed to reduce the circulation from 95% of Γ_0 to 50% of Γ_0. The maximum circulation transfer for case 1 is 82% higher, and the reconnection time is 25% smaller than case 0.

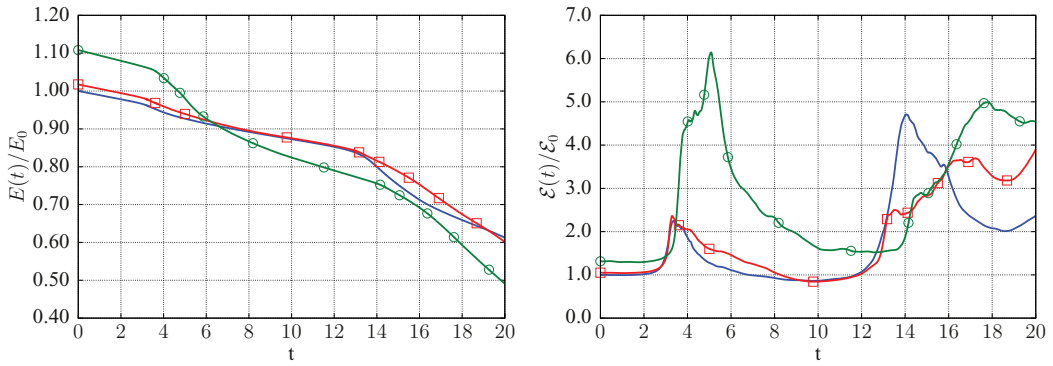

FIG. 13. Evolution of energy (left) and enstrophy (right) over time, normalized by their initial values for the case without initial axial flow. Case 0 (no symbols—blue online), case 1 (squares—red online), and case 2 (circles—green online).

The energy spectrum during this collision, as well as during the subsequent collision between the elliptical vortex rings (not shown in Figure 12) exhibits a persistent power-law regime with $-7/3$ slope (Figure 15) that is further discussed in Sec. IV C.

We mention that in Ref. 47 the role of axial flow in the breakup of vortex structures is studied for an experimental vortex ring at $Re = 1600$. The breakup in that study differs however from the breakup observed in ours (both cases 1 and 2). The breakup in our results is dominated by a Kelvin-Helmholtz instability originating from anti-parallel axial flows, whereas the breakup of the vortex ring in Ref. 47 is dominated by waves amplified by the Widnall instability, together with an induced uniaxial axial flow. That is, our breakup is dominated by shear, whereas theirs by compression of vortex lines.

B. Case 2: $q = 0.958$

The shearing of the vortex sheet during the first collision observed in case 1 is even more pronounced in case 2, due to the increased axial flow strength. Again the sheet undergoes rapid instability and the small-scale vortical structures get rapidly advected downstream. This can be seen in Figure 12 as clusters of small-scale vorticity structures swirling around each of the main tubes. The related smaller localization of strong vorticity is visible in the diminished value of the maximum vorticity of case 2 with respect to case 1 (Figure 14, right), and the much higher enstrophy values (Figure 13, right).

Table I shows that the reconnection time and the maximum circulation transfer rate for case 2 are between those for case 0 and case 1. The onset time for reconnection as well as the time of

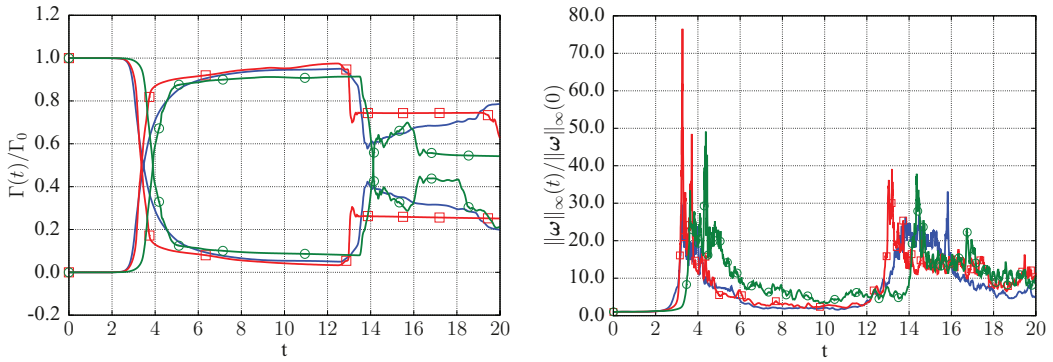

FIG. 14. (Left) Circulation in half of the $x = 0$ and $z = 0$ planes as a function of time, normalized by the circulation in the $z = 0$ plane at $t = 0$. (Right) Evolution of maximum vorticity over time, normalized by the vorticity at $t = 0$. Case 0 (no symbols—blue online), case 1 (squares—red online), and case 2 (circles—green online).

TABLE I. Comparison of several characteristic reconnection quantities with varying axial flow strength.

Flow case	$\max \mathrm{d}\Gamma^*/\mathrm{d}t$	$t_{\mathrm{d}\Gamma^*/\mathrm{d}t,\max}$	$t_{0.95}$	$t_{0.5}$	t_R
0	1.042	3.07	2.86	3.46	0.60
1	1.901	3.20	2.91	3.37	0.45
2	1.649	3.63	3.37	3.89	0.52

maximum circulation rate are both delayed with respect to the previous cases. Furthermore, Figure 14 (left plot) shows that the circulation transfer is smaller than for both case 0 and case 1, as the circulation transfer flattens out at $t \approx 5$.

Again we find a power-law regime in the energy spectrum with $-7/3$ slope (Figure 15), which will be further discussed in Sec. IV C.

C. Energy spectrum

The $-7/3$ energy spectrum characterizes the second collision of vortex reconnection without any initial axial flow (case 0) (Figure 3, right), as well as the first and second collisions of vortex reconnection, for both cases 1 and 2, with imposed initial axial flow (Figure 15). In both cases the common characteristic is the presence of axial flow during the collision of the vortex structures.

We remark that the $-7/3$ energy spectrum has been associated with a cascade of energy dictated solely by the rate of helicity transfer, η. In Brissaud *et al.*,[54] based on dimensional analysis, it is argued that in a flow with energy dissipation rate $\varepsilon = 0$ and helicity dissipation rate $\eta \neq 0$, the spectra of energy and helicity in the inertial range have the form

$$E(k) \sim \eta^{2/3} k^{-7/3}, \tag{10}$$

$$H(k) \sim \eta^{2/3} k^{-4/3}. \tag{11}$$

This is referred to as the pure helicity cascade or direct helicity cascade, and is contrasted with the case of a joint cascade of energy and helicity, where $\eta \neq 0$ and $\varepsilon \neq 0$, such that

$$E(k) \sim \varepsilon^{2/3} k^{-5/3}, \tag{12}$$

$$H(k) \sim \eta \varepsilon^{-1/3} k^{-5/3}. \tag{13}$$

Numerical computations have not shown the existence of the pure helicity cascade in isotropic homogeneous turbulence, instead the simultaneous cascade of energy and helicity has consistently

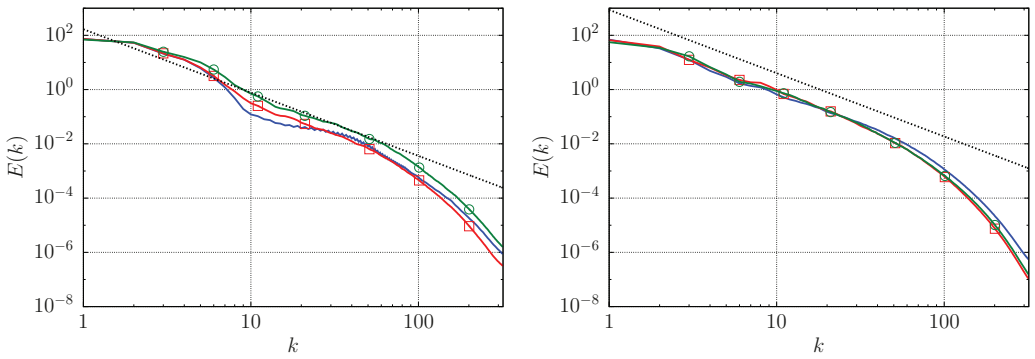

FIG. 15. Three-dimensional energy spectrum of case 0 (no symbols—blue online), case 1 (squares—red online), and case 2 (circles—green online) at $t = 3.8$ (left) and $t = 15.5$ (right). The dashed line in both plots corresponds to a $-7/3$ slope.

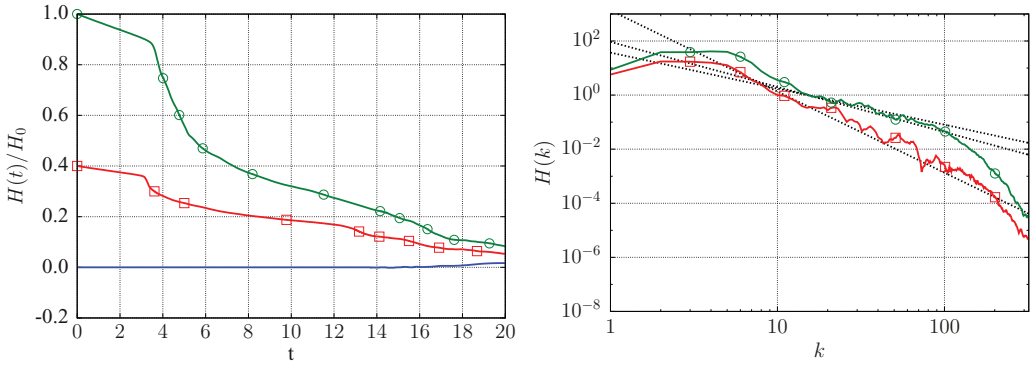

FIG. 16. Helicity for all three cases, normalized by its value at $t = 0$ for case 2 (left). Helicity spectrum at $t = 3.8$ for cases 1 and 2, black dashed lines are $-4/3$, $-5/3$, and -3 slopes (right). Case 0 (no symbols—blue online), case 1 (squares—red online), and case 2 (circles—green online).

been found.[49,55,56] In an experimental study on vortex bursts in a laminar flow,[57] the time-averaged velocity spectrum downstream from the burst region seems to develop a slope close to $-7/3$ (Figure 4 in Ref. 57), although this development is not mentioned by the authors.

For all three simulations discussed here, we have plotted the helicity $H(t) = \int_V \mathbf{u} \cdot \boldsymbol{\omega}\, \mathrm{d}V$ in Figure 16. For vortex reconnection without initial axial flow, the helicity deviates from zero after $t \approx 13$, which coincides with the time when the $-7/3$ slope first appears. In order to examine this correlation we have repeated the case 0 computation in one-fourth of the computational box, using symmetric boundary conditions to ensure zero helicity at all times, and still find the $-7/3$ slope in the energy spectrum during the second collision.

We computed the helicity spectrum for cases 1 and 2 during the first collision. For case 0, the helicity is close to zero, therefore the helicity spectrum integrates to a value close to zero. The definition of an inertial range for the helicity spectrum is thus not meaningful in this case. For cases 1 and 2 the helicity is positive and the spectrum at $t = 3.8$ is shown in Figure 16 (right). Due to oscillations in the spectrum, the slope cannot be conclusively identified: for case 1 the slope is around -3 whereas for case 2 the slope can be interpreted both as $-4/3$ or $-5/3$.

We conclude this discussion by noting that in our simulations, the energy dissipation rate is $\varepsilon > 0$ at all times, which should exclude the direct helicity cascade possibility.[54] The results and the above discussion do not conclusively explain the $-7/3$ energy spectrum slope and its relationship to helicity in turbulent flows, which remains a subject for further study.

V. CONCLUSIONS

We have performed long-time direct numerical simulations of the reconnection of two anti-parallel vortex tubes at $Re = 10\,000$ with and without initial axial flow. The collision process is described through visualizations of the vortex structures as well as the corresponding energy spectra. The present simulations demonstrate the imparting of an axial flow on the vortex structures formed after the first collision, that largely influences the subsequent collision that is here revealed for the first time.

Vortex reconnection without initial axial flow exhibits a $-5/3$ slope in the energy spectrum during the first collision, as well as a constant-slope energy decay after the collision—both features commonly associated with turbulent flows. The threads of this collision undergo an interaction of their own which is dominated by diffusion due to their low Re. The elliptical vortex rings resulting from the first collision undergo a full oscillation due to axis-switching before they collide, with a burst of small-scale vortical structures. The repeated vortex collisions exhibit features common to turbulent flows, supporting the notion that reconnection events play an important role in the dynamics of turbulent flows. The present simulations do not show however a vortex reconnection cascade, due to the small circulation of the threads and their susceptibility to instabilities. This observation

challenges the suggestion that a vortex reconnection cascade could actually be realized, even at initial *Re* much larger than 10 000.

The present simulations elucidate also the role of axial flow in vortex collision dynamics. In the case of non-initial axial flow, upon the first collision, elliptical vortex rings are formed and the coiled vortex lines connecting the rings to the threads impart an axial flow inside their cores, directed away from the connection region. During the evolution of the elliptical vortex rings we observe repeated axis-switching accordingly associated with changes in the direction of the axial flow. This axial flow determines the dynamics of the subsequent vortex ring collision that results in a multitude of strong albeit small-scale vortical structures. We wish to stress the notion that reconnection between structures without axial flow leads to structures with axial flow as this may be highly relevant to vortex dynamics of turbulent flows.

Adding an initial axial flow to the vortex tubes, with a swirl number of $q = 0.383$, was found to decrease the reconnection time and increase the rate of maximum circulation transfer, while the main flow structures and global diagnostics remain largely unchanged. Further increasing the swirl number to $q = 0.958$ leads to a rapid breakup of the vortex sheet formed at the onset of the collision. Our simulations show the occurrence of a $-7/3$ energy spectrum for a high Reynolds number vortex collision with non-zero axial flow. The possible relationship of this spectrum to helical turbulent flows and in particular the pure helicity cascade remains subject to further research.

Further work involves studies at higher Reynolds numbers, in order to examine the possibility of a reconnection cascade, using wavelet adapted multi-resolution particle methods.[58]

ACKNOWLEDGMENTS

This work was supported by a grant from the Swiss National Supercomputing Centre (CSCS) under project s70. We wish to thank Jean Favre at CSCS (Switzerland) for his assistance with visualization.

[1] A. K. M. F. Hussain, "Coherent structures—reality and myth," Phys. Fluids **26**, 2816–2850 (1983).
[2] R. S. Scorer and L. J. Davenport, "Contrails and aircraft downwash," J. Fluid Mech. **43**, 451–464 (1970).
[3] S. Crow, "Stability theory for a pair of trailing vortices," AIAA J. **8**, 2172–2179 (1970).
[4] A. Pumir and E. D. Siggia, "Vortex dynamics and the existence of solutions to the Navier-Stokes equations," Phys. Fluids **30**, 1606–1626 (1987).
[5] R. M. Kerr, "Evidence for a singularity of the 3-dimensional, incompressible Euler equations," Phys. Fluids A **5**, 1725–1746 (1993).
[6] T. Hou and R. Li, "Computing nearly singular solutions using pseudo-spectral methods," J. Comput. Phys. **226**, 379–397 (2007).
[7] T. Y. Hou and R. Li, "Blowup or no blowup? the interplay between theory and numerics," Physica D **237**, 1937–1944 (2008).
[8] T. Hou and Z. Lei, "On the stabilizing effect of convection in three-dimensional incompressible flows," Commun. Pure Appl. Math. **62**, 0501–0564 (2009).
[9] T. Fohl and J. S. Turner, "Colliding vortex rings," Phys. Fluids **18**, 433–436 (1975).
[10] Y. Oshima and S. Asaka, "Interaction of two vortex rings moving side by side," *Nature Science Report* (Ochanomizu University, 1975), Vol. 1.
[11] P. R. Schatzle, "An experimental study of fusion of vortex rings," Ph.D. dissertation (California Institute of Technology, Pasadena, CA, 1987).
[12] Y. Oshima and N. Izutsu, "Cross-linking of two vortex rings," Phys. Fluids **31**, 2401–2403 (1988).
[13] W. T. Ashurst and D. I. Meiron, "Numerical study of vortex reconnection," Phys. Rev. Lett. **58**, 1632–1635 (1987).
[14] S. Kida, M. Takaoka, and F. Hussain, "Reconnection of two vortex rings," Phys. Fluids A **1**, 630–632 (1989).
[15] H. Aref and I. Zawadzki, "Linking of vortex rings," Nature (London) **354**, 50–53 (1991).
[16] S. Kida, M. Takaoka, and F. Hussain, "Collision of two vortex rings," J. Fluid Mech. **230**, 583–646 (1991).
[17] A. Pumir and R. M. Kerr, "Numerical simulation of interacting vortex tubes," Phys. Rev. Lett. **58**, 1636–1639 (1987).
[18] M. V. Melander and F. Hussain, "Cut-and-connect of two antiparallel vortex tubes," in *Proceedings of the 1988 CTR Summer Program* (Stanford University, 1988), pp. 257–286.
[19] R. M. Kerr and F. Hussain, "Simulation of vortex reconnection," Physica D **37**, 474–484 (1989).
[20] M. J. Shelley, D. I. Meiron, and S. A. Orszag, "Dynamical aspects of vortex reconnection of perturbed anti-parallel vortex tubes," J. Fluid Mech. **246**, 613–652 (1993).
[21] M. V. Melander and N. J. Zabusky, "Interaction and 'apparent' reconnection of 3d vortex tubes via direct numerical simulations," Fluid Dyn. Res. **3**, 247–250 (1988).
[22] N. J. Zabusky and M. V. Melander, "Three-dimensional vortex tube reconnection: morphology for orthogonally-offset tubes," Physica D **37**, 555–562 (1989).

[23] N. J. Zabusky, O. N. Boratav, R. B. Pelz, M. Gao, D. Silver, and S. P. Cooper, "Emergence of coherent patterns of vortex stretching during reconnection: a scattering paradigm," Phys. Rev. Lett. **67**, 2469–2472 (1991).
[24] O. N. Boratav, R. B. Pelz, and N. J. Zabusky, "Reconnection in orthogonally interacting vortex tubes: direct numerical simulations and quantifications," Phys. Fluids A **4**, 581–605 (1992).
[25] S. Kida and M. Takaoka, "Reconnection of vortex tubes," Fluid Dyn. Res. **3**, 257–261 (1988).
[26] P. Chatelain, D. Kivotides, and A. Leonard, "Reconnection of colliding vortex rings," Phys. Rev. Lett. **90**, 054501 (2003).
[27] Y. Oshima, "Head-on collision of two vortex rings," J. Phys. Soc. Jpn **44**, 328–331 (1978).
[28] T. Kambe and T. Minota, "Acoustic wave radiated by head-on collision of two vortex rings," Proc. R. Soc. London, Ser. A. **386**, 277–308 (1983).
[29] S. Stanaway, K. Shariff, and F. Hussain, "Head-on collision of viscous vortex rings," in *Proceedings of the 1988 CTR Summer Program* (Stanford University, 1988), pp. 287–309.
[30] T. T. Lim and T. B. Nickels, "Instability and reconnection in the head-on collision of two vortex rings," Nature (London) **357**, 225–227 (1992).
[31] C.-C. Chu, C.-T. Wang, C.-C. Chang, R.-Y. Chang, and W.-T. Chang, "Head-on collision of two coaxial vortex rings: experiment and computation," J. Fluid Mech. **296**, 39–71 (1995).
[32] P. G. Saffman, "A model of vortex reconnection," J. Fluid Mech. **212**, 395–402 (1990).
[33] S. Kida, "Vortex reconnection," Annu. Rev. Fluid Mech. **26**, 169–189 (1994).
[34] F. Hussain and K. Duraisamy, "Mechanics of viscous vortex reconnection," Phys. Fluids **23**, 021701 (2011).
[35] P. Koumoutsakos, "Inviscid axisymmetrization of an elliptical vortex," J. Comput. Phys. **138**, 821–857 (1997).
[36] P. Koumoutsakos, "Multiscale flow simulations using particles," Annu. Rev. Fluid Mech. **37**, 457–487 (2005).
[37] I. Sbalzarini, J. Walther, M. Bergdorf, S. E. Hieber, E. M. Kotsalis, and P. Koumoutsakos, "PPM—a highly efficient parallel particle-mesh library," J. Comput. Phys. **215**, 566–588 (2006).
[38] M. Bergdorf, P. Koumoutsakos, and A. Leonard, "Direct numerical simulations of vortex rings at $Re_\Gamma = 7,500$," J. Fluid Mech. **581**, 495–505 (2007).
[39] P. Chatelain, A. Curioni, M. Bergdorf, D. Rossinelli, W. Andreoni, and P. Koumoutsakos, "Billion vortex particle direct numerical simulations of aircraft wakes," Comput. Methods Appl. Mech. Eng. **197**, 1296–1304 (2008).
[40] W. M. van Rees, A. Leonard, D. Pullin, and P. Koumoutsakos, "A comparison of vortex and pseudospectral methods for the simulation of periodic vortical flows at high Reynolds numbers," J. Comput. Phys. **230**, 2794–2805 (2011).
[41] D. Virk, F. Hussain, and R. M. Kerr, "Compressible vortex reconnection," J. Fluid Mech. **304**, 47–86 (1995).
[42] G. F. Carnevale, M. Briscolini, R. C. Kloosterziel, and G. K. Vallis, "Three-dimensionally perturbed vortex tubes in a rotating flow," J. Fluid Mech. **341**, 127–163 (1997).
[43] G. Winckelmans and A. Leonard, "Contributions to vortex particle methods for the computation of three-dimensional incompressible unsteady flows," J. Comput. Phys. **109**, 247–273 (1993).
[44] A. N. Kolmogorov, "On the degeneration of isotropic turbulence in an incompressible viscous fluid," Dokl. Akad. Nauk SSSR **33**, 538–541 (1941).
[45] M. Lesieur, *Turbulence in Fluids*, 4th ed. (Springer, Dordrecht, 2008).
[46] M. R. Dhanak and B. De Bernadinis, "The evolution of an elliptic vortex ring," J. Fluid Mech. **109**, 189–216 (1981).
[47] T. Naitoh, N. Fukuda, T. Gotoh, H. Yamada, and K. Nakajima, "Experimental study of axial flow in a vortex ring," Phys. Fluids **14**, 143–149 (2002).
[48] H. Moses, "Eigenfunctions of the curl operator, rotationally invariant Helmholtz theorem, and applications to electromagnetic theory and fluid mechanics," SIAM J. Appl. Math. **21**, 114–144 (1971).
[49] Q. Chen, S. Chen, and G. L. Eyink, "The joint cascade of energy and helicity in three-dimensional turbulence," Phys. Fluids **15**, 361–374 (2003).
[50] M. V. Melander and F. Hussain, "Polarized vorticity dynamics on a vortex column," Phys. Fluids A **5**, 1992–2003 (1993).
[51] D. Virk, M. V. Melander, and F. Hussain, "Dynamics of a polarized vortex ring," J. Fluid Mech. **260**, 23–55 (1994).
[52] J. S. Marshall, P. Brancher, and A. Giovannini, "Interaction of unequal anti-parallel vortex tubes," J. Fluid Mech. **446**, 229–252 (2001).
[53] J. M. Ortega, R. L. Bristol, and O. Savas, "Experimental study of the instability of unequal-strength counter-rotating vortex pairs," J. Fluid Mech. **474**, 35–84 (2003).
[54] A. Brissaud, U. Frisch, J. Leorat, M. Lesieur, and A. Mazure, "Helicity cascades in fully developed isotropic turbulence," Phys. Fluids **16**, 1366–1367 (1973).
[55] V. Borue and S. A. Orszag, "Spectra in helical three-dimensional homogeneous isotropic turbulence," Phys. Rev. E **55**, 7005–7009 (1997).
[56] P. D. Mininni and A. Pouquet, "Rotating helical turbulence. I. global evolution and spectral behavior," Phys. Fluids **22**, 035105 (2010).
[57] Y. Cuypers, A. Maurel, and P. Petitjeans, "Vortex burst as a source of turbulence," Phys. Rev. Lett. **91**, 194502 (2002).
[58] M. Bergdorf and P. Koumoutsakos, "A Lagrangian particle-wavelet method multiscale modeling and simulation," Multiscale Model. Simulat. **5**(3), 980–995 (2006).